Results of an explorative clinical evaluation suggest immediate and persistent post-reperfusion metabolic paralysis drives kidney ischemia reperfusion injury

Lindeman, J.H.; Wijermars, L.G.; Kostidis, S.; Mayboroda, O.A.; Harms, A.C.; Hankemeier, T.; ... ; Bakker, J.A.

Results of an explorative clinical evaluation suggest immediate and persistent post-reperfusion metabolic paralysis drives kidney ischemia reperfusion injury

OPEN

Jan H. Lindeman[1], Leonie G. Wijermars[1], Sarantos Kostidis[2], Oleg A. Mayboroda[2], Amy C. Harms[3], Thomas Hankemeier[3], Jörgen Bierau[4], Karthick B. Sai Sankar Gupta[5], Martin Giera[2], Marlies E. Reinders[6], Melissa C. Zuiderwijk[1,7], Sylvia E. Le Dévédec[7], Alexander F. Schaapherder[1] and Jaap A. Bakker[8]

[1]Department of Surgery, Leiden University Medical Centre, Leiden, Netherlands; [2]Department of Center for Proteomics and Metabolomics, Leiden University Medical Centre, Leiden, Netherlands; [3]Department of Analytical BioSciences, Leiden Academic Centre for Drug Research, Leiden University, Leiden, The Netherlands; [4]Department of Clinical Genetics, Maastricht University Medical Centre, Maastricht, The Netherlands; [5]Leiden Institute of Chemistry, Leiden University, Leiden, The Netherlands; [6]Department of Medicine, Leiden University Medical Centre, Leiden, Netherlands; [7]Department of Division of Toxicology, Leiden Academic Centre for Drug Research, Leiden University, Leiden, The Netherlands; and [8]Department of Clinical Chemistry & Laboratory Medicine, Leiden University Medical Centre, Leiden, Netherlands

Delayed graft function is the manifestation of ischemia reperfusion injury in the context of kidney transplantation. While hundreds of interventions successfully reduce ischemia reperfusion injury in experimental models, all clinical interventions have failed. This explorative clinical evaluation examined possible metabolic origins of clinical ischemia reperfusion injury combining data from 18 pre- and post-reperfusion tissue biopsies with 36 sequential arteriovenous blood samplings over the graft in three study groups. These groups included living and deceased donor grafts with and without delayed graft function. Group allocation was based on clinical outcome. Magic angle NMR was used for tissue analysis and mass spectrometry-based platforms were used for plasma analysis. All kidneys were functional at one-year. Integration of metabolomic data identified a discriminatory profile to recognize future delayed graft function. This profile was characterized by post-reperfusion ATP/GTP catabolism (significantly impaired phosphocreatine recovery and significant persistent (hypo)xanthine production) and significant ongoing tissue damage. Failing high-energy phosphate recovery occurred despite activated glycolysis, fatty-acid oxidation, glutaminolysis and autophagia, and related to a defect at the level of the oxoglutarate dehydrogenase complex in the Krebs cycle. Clinical delayed graft function due to ischemia reperfusion injury associated with a post-reperfusion metabolic collapse. Thus, efforts to quench delayed graft function due to ischemia reperfusion injury should focus on conserving metabolic competence, either by preserving the integrity of the Krebs cycle and/or by recruiting metabolic salvage pathways.

Kidney International (2020) **98,** 1476–1488; https://doi.org/10.1016/j.kint.2020.07.026

KEYWORDS: ATP; delayed graft function; glycolysis; ischemia reperfusion injury; metabolism; oxidative phosphorylation

Translational Statement

This study shows that delayed graft function (graft ischemia reperfusion injury) is preceded by a post-reperfusion metabolic collapse, which leads to an inability to sustain the organ's energy requirements. Efforts aimed at quenching delayed graft function (and ischemia reperfusion injury in general) should aim to preserve or restore metabolic competence.

Ischemia reperfusion injury (IRI) is the phenomenon of increased tissue damage after reperfusion of previously ischemic tissue.[1,2] It is a main contributor to organ damage after myocardial or brain infarction[3] and graft damage after organ transplantation.[4] Although myriad interventions quench IRI in preclinical models, clinical success remains to be achieved.[3,4] Thus, there appears a translational gap between preclinical models and the clinical context.

Delayed graft function (DGF) is the manifestation of IRI in the setting of kidney transplantation.[5] DGF is defined as the need for dialysis in the first week or weeks after transplantation.[6] Although DGF is extremely rare in the context of living-donor graft procedures, it affects up to 90% of deceased donor graft transplantations.[6] Previous work demonstrated

Correspondence: *Jan H. Lindeman, Department of Surgery, Leiden University Medical Center, P.O. Box 9600, 2300 RC Leiden, The Netherlands. E-mail: Lindeman@lumc.nl*

Received 20 January 2020; revised 8 June 2020; accepted 2 July 2020; published online 8 August 2020

an association between incident DGF and post-reperfusion normoxic glycolysis.[7] This observation implies that DGF relates to a defect in graft energy homeostasis as result of mitochondrial dysfunction in the reperfusion phase.[7] On this basis, we hypothesized that clinical DGF involves and may be driven by a metabolic defect (or defects). The objective of this study was to perform an in-depth analysis of metabolic responses to ischemia-reperfusion with and without IRI (DGF).

This explorative metabolic evaluation is based on an integrated, time-resolved approach that involved sequential assessment of arteriovenous concentration (AV) differences over reperfused grafts and parallel profiling of graft (tissue) biopsies. Three study groups were included: grafts from deceased donor grafts with and without later IRI and living donor grafts. Group allocation of deceased donor grafts (+DGF and –DGF, respectively) was done retrospectively on basis of their clinical outcome. Living donor grafts were included as a reference because these grafts associate with an instantaneous functional recovery following reperfusion. To cover the primary aspects of metabolic homeostasis, the focus in this study was on the following gross metabolic clusters: nucleotide triphosphate metabolism, fatty acid (β)–oxidation, glycolysis/glutaminolysis, autophagy, Krebs cycle (defects), and cell damage. The data are presented accordingly.

RESULTS

The study sample included 53 patients. Paired tissue biopsies were obtained from 18 patients, and sequential AV sampling was performed in 36 patients. One patient had both biopsies taken and underwent AV sampling. Clinical details for the 3 study groups are shown in Supplementary Table S1A (tissue biopsies) and S1B (AV sampling). All DGF cases required multiple dialyses over a time course of at least 7 days, and all showed adequate functional recovery. None of the deceased donors without DGF required dialysis after transplantation. One-year graft survival was 100%.

We first explored putative differences in metabolic signatures for the 3 donor groups (the living [reference] donor grafts, the –DGF deceased donor grafts, and +DGF [IRI] deceased donor grafts) by mapping the plasma metabolome (AV differences) for the 30-minutes post-reperfusion time point (Figure 1a) and the tissue metabolome (tissue biopsies) for the 40-minutes post-reperfusion time point (Figure 1b). These time points were chosen to avoid interference from washout of metabolites that accumulated during ischemia or cold storage, or that were constituents of the preservation fluid (e.g., histidine washout from living donor grafts; Supplementary Figure S1 shows the selective use of H [Histidine] TK preservation fluid in these grafts).[7] Results (z-scores) for these time points are summarized in the heat maps in Figure 1a (AV differences) and 1b (tissue). Grouping of the data was performed according to the 6 clusters that cover all metabolic data: (i) nucleoside triphosphate catabolism, (ii) β-oxidation, (iii) glycolysis/glutaminolysis, (iv) autophagy, (v) Krebs cycle defects, and (vi) cell damage.

Heat maps for the AV differences indicate parallel metabolic signatures for the living donor and –DGF grafts, and a clearly distinctive signature for the +DGF grafts (Figure 1a). A similar, although less pronounced, pattern was observed for the tissue metabolites (Figure 1b). Exclusive mapping of –DGF and +DGF grafts (without the living donor graft) resulted in similar conclusions (not shown), indicating that inclusion of the living donor (reference) data in the analysis did not interfere with the conclusions of the analysis. Collectively, the data provide a gross metabolic signature for renal IRI.

For the sake of clarity, the data of the individual metabolites are presented in terms of the 6 metabolic clusters. To avoid interference from the initial washout of metabolites that have accumulated during cold storage within the first minutes of reperfusion, estimations for net post-perfusion release or uptake are based on integration of AV differences for the 10- to 30-minutes post-reperfusion time intervals (area between the curves).

The first cluster of metabolites ("nucleoside triphosphate catabolism") signals a persistent post-reperfusion metabolic incompetence ("power shutdown") in grafts with later DGF (+DGF). This conclusion is based on impaired post-reperfusion recovery of the high-energy phosphate-buffer phosphocreatine in +DGF grafts ($P < 0.001$; Figure 2a), and by persistent post-reperfusion adenosine triphosphate/guanosine triphosphate (ATP/GTP) catabolism. The latter is reflected in the continued release (AV differences) of hypoxanthine and xanthine (Figure 2b and c, $P < 0.0001$ and 0.02, respectively), the terminal degradation products of ATP and GTP from these grafts. Data for the pre-reperfusion tissue biopsies showed graded degrees of inosine and hypoxanthine accumulation at the end ischemic storage period, with the lowest content found in living and the highest in deceased donor grafts (Figure 2d and e). Post-reperfusion ($t = 40$ min) hypoxanthine and inosine tissue contents were similar and low in all 3 donor groups (Figure 2d and e).

Post-reperfusion ATP catabolism in +DGF grafts occurred despite an apparent post-reperfusion restoration of fatty acid β-oxidation (Supplementary Figure S2), activated glycolysis/glutaminolysis (Figure 3), and autophagy (Figure 4). All 3 graft types showed uniform restoration of tissue β-hydroxybutyrate content (Supplementary Figure S2A) and selective clearance (uptake) of medium-chain fatty acids (C8–C12) from the circulation (Supplementary Figures S1 and S2B–E), indicating uniform reinstatement of β-oxidation. However, tissue accumulation of acetyl-carnitine in the –DGF and +DGF deceased donor grafts (Supplementary Figure S2F), and washout (AV differences) of acetyl-carnitine from +DGF grafts (Supplementary Figure S2G, $P < 0.03$) imply graded defects in disposal of acetyl groups formed during β-oxidation in –DGF and +DGF deceased donor grafts.

Mapping of glycolysis/glutaminolysis networks (Figure 3) showed equal tissue glucose levels (Figure 4a) and confirmed persistent post-reperfusion normoxic glycolysis as an

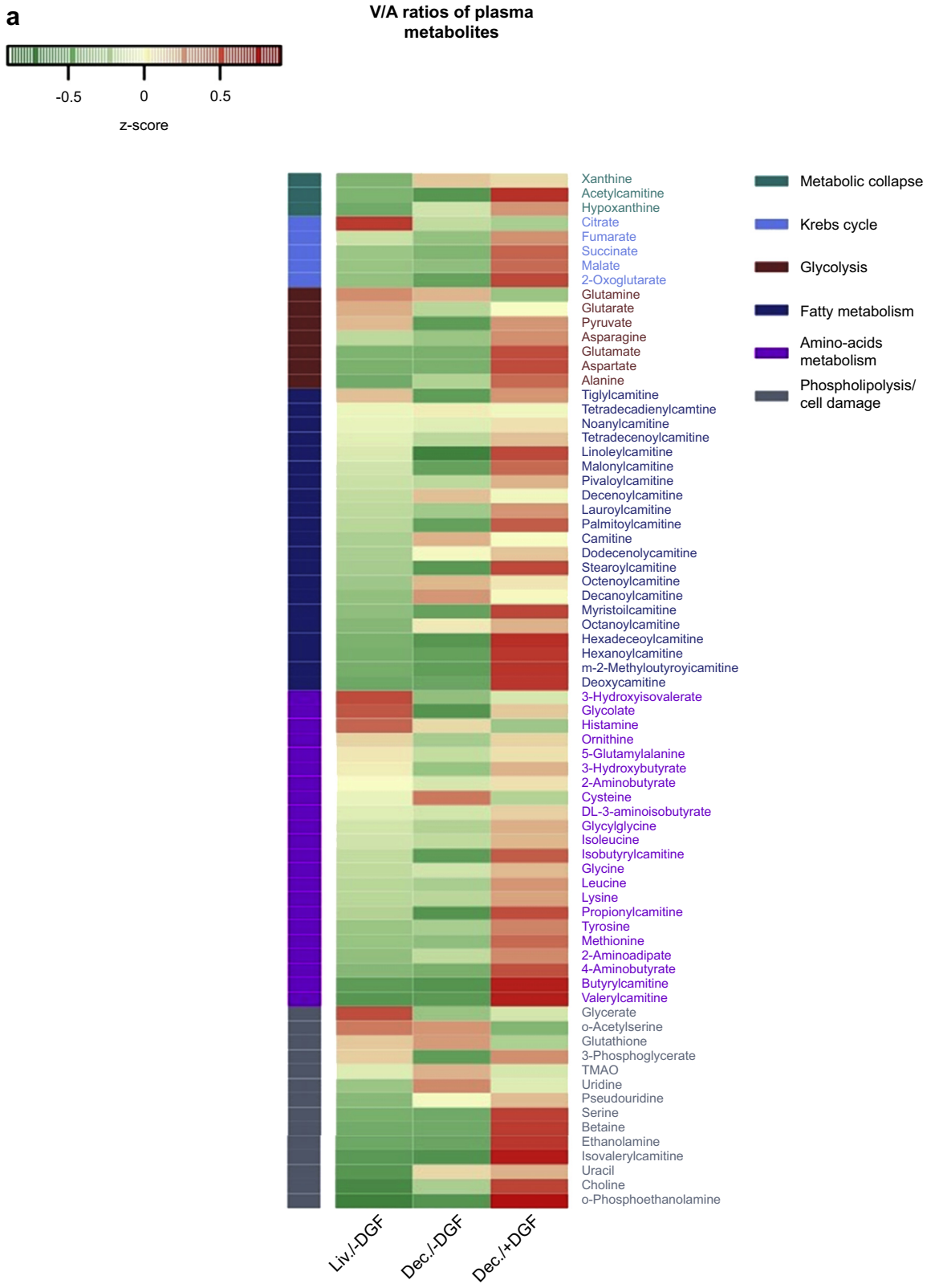

Figure 1 | Clustered heat maps for the arterial-venous metabolite concentration differences over the donor graft at 30 minutes and tissue metabolite contents 40 minutes after reperfusion. (**a**) Clustered heat map for the arterial-venous metabolite concentrations at t = 30 minutes after reperfusion. The columns represent the 3 donor groups (living donor grafts [reference group, *n* = 10]; deceased donor grafts without later delayed graft function [DGF {–DGF, *n* = 10}], and deceased donor grafts with later DGF [+DGF, *n* = 16]). Compounds are clustered according to the 5 metabolic clusters and, within each cluster, ranked based on the z-score of the living donors group. Green reflects net uptake by the graft and red reflects the net release from the graft. (Continued)

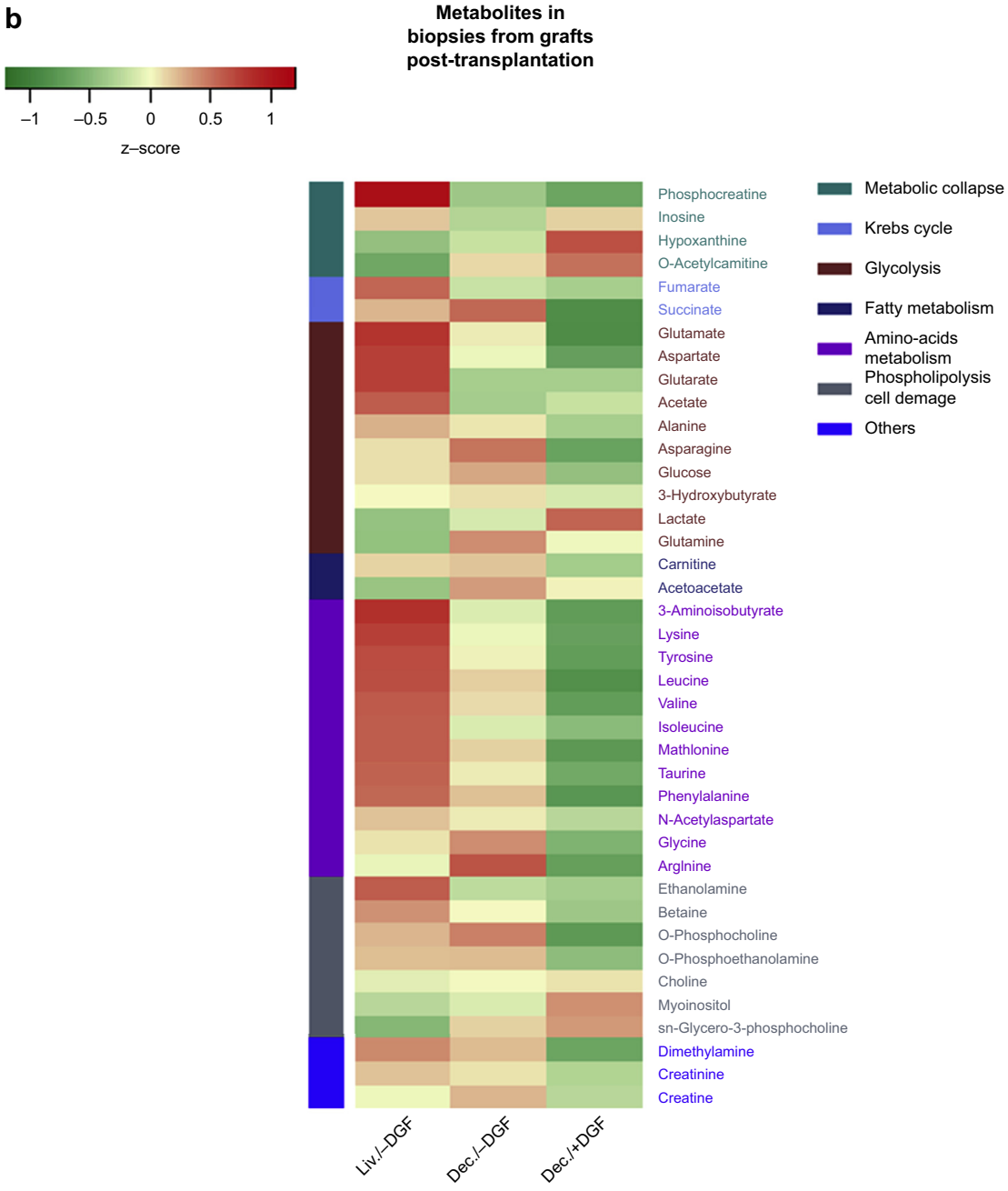

Figure 1 (Continued) (**b**) Clustered heat map for tissue metabolites identified in the HR magic angle nuclear magnetic resonance analysis of graft biopsies taken 40 minutes after reperfusion. The columns represent the 3 donor groups (living donor group [reference group, $n = 6$, deceased donor grafts without later DGF [–DGF, $n = 6$], and deceased donor grafts with later DGF [+DGF, $n = 6$]). Red reflects a tissue content above and green reflects a tissue content below the geometric mean of the 3 groups.

exclusive feature of +DGF donor grafts (viz. persistent lactate and pyruvate release (Figure 3b and c, $P < 0.0001$ and < 0.04, respectively) and release of the transamination products alanine and aspartate (Figure 3e and f, $P < 0.02$ and < 0.0001, respectively). Serine (Figure 4b) and phosphoserine (Supplementary Figure 3D) release from +DGF grafts may (partially) reflect transamination of the glycolysis intermediate phosphoglycerate. Persistent post-reperfusion glutamate release (Figure 3k, $P < 0.002$), selective release of the transamination products alanine and aspartate (Figure 3e and f), and exhaustion of the tissue asparagine pool (Figure 3j, $P < 0.03$) in +DGF grafts imply continued post-reperfusion glutaminolysis (alanine) and glutamine shuttling (asparagine-aspartate)[8] in the post-reperfusion phase of these grafts. Moreover, exclusive release of serine, methionine, and tyrosine (Figure 4a–c, all Ps < 0.0005), along with disposal of

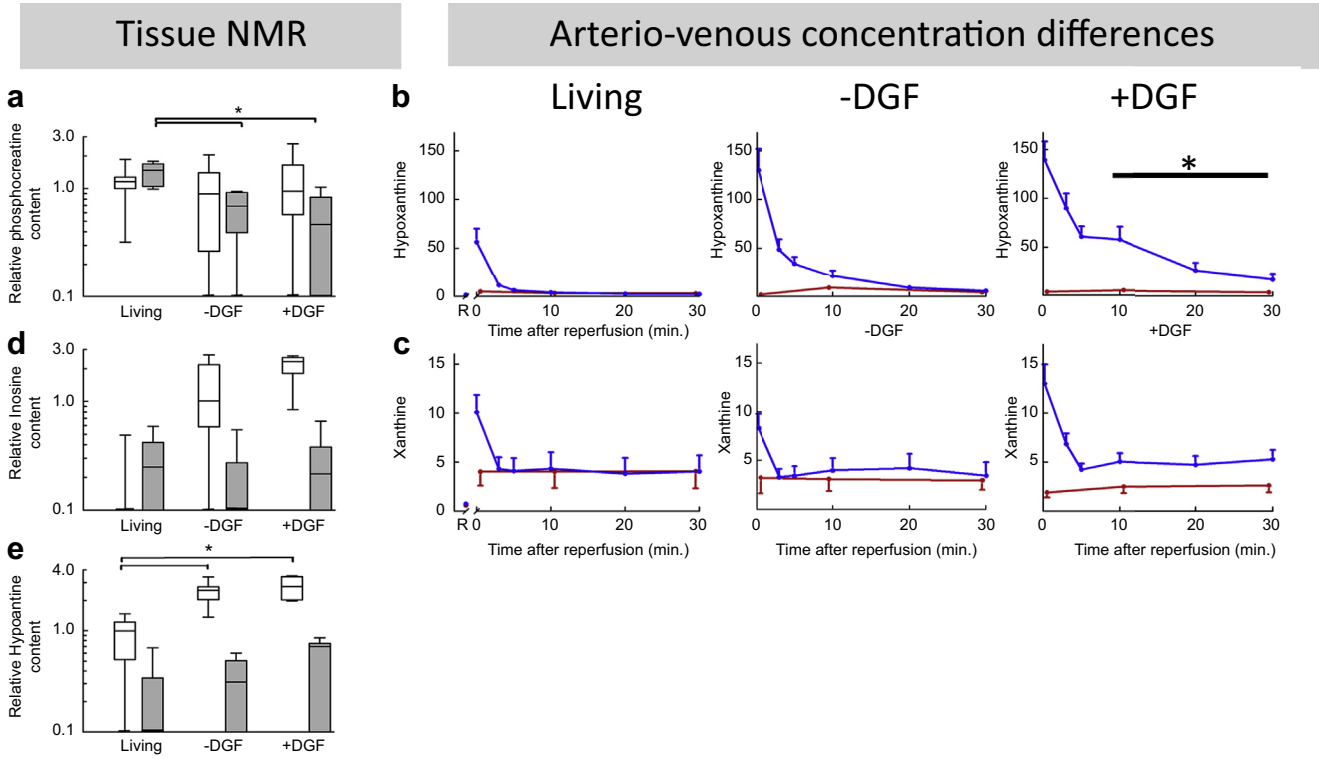

Figure 2 | Post-reperfusion high-energy phosphate catabolism associates with future delayed graft function (DGF). Curves for the arterial-venous concentration (AV) differences (red curve is arterial; blue curve is venous). Tissue biopsies (bar graphs): white bars represent pre-reperfusion biopsies; gray bars represent post-reperfusion biopsies (t = 40 min after reperfusion). *$P < 0.05$. (**a**) Pre- and post-reperfusion tissue phosphocreatine content in the 3 donor groups (living donor, $n = 6$), deceased donor grafts without later DGF (–DGF, $n = 6$), and deceased donor grafts with later DGF (+DGF, $n = 6$). Impaired post-reperfusion tissue phosphocreatine recovery in –DGF and +DGF grafts ($P < 0.001$ and $P < 0.004$, respectively). (**b,c**) Post-reperfusion arterial (red) and venous (blue) blood concentrations for (**b**) hypoxanthine and (**c**) xanthine, the end products of nucleoside triphosphate catabolism. Immediate post-reperfusion washout of accumulated hypoxanthine and xanthine for all study groups ($n = 10$, 10, and 16 in the living, –DGF, and +DGF groups, respectively). Persistent hypoxanthine and xanthine release from +DGF grafts ($P < 0.0001$ and $P < 0.02$, respectively) implies persistent nucleoside triphosphate catabolism in +DGF grafts. Note: Reference (R) in the living graft graphs depicts arterial (red) and venous (blue) plasma contents sampled over normal kidneys. *P* values are for the AV difference in the 10- and 30-minute interval. (**d,e**) Progressive degrees of pre-reperfusion (white bars) inosine and hypoxanthine accumulation imply graded adenosine triphosphate catabolism during organ procurement of living-donor and deceased-donor grafts ($P < 0.008$ and $P < 0.004$, respectively). NMR, nuclear magnetic resonance.

butyrylcarnitine and isovalerylcarnitine (Figure 4d and e, $P < 0.006$ and < 0.003, respectively), deamination products of the branched chain amino acids[9,10] from +DGF grafts, but not from the other graft types (Figure 4a–e), implies post-reperfusion autophagy in these grafts.[11]

Post-reperfusion acetyl-carnitine accumulation (tissue) in –DGF and +DGF grafts (Figure 2f) and initial (living donor and –DGF grafts) and continued (+DGF grafts) acetyl-carnitine release ($P < 0.03$) indicate a transient (–DGF grafts) or persistent (+DGF grafts) impaired acetyl-coenzyme A disposal after reperfusion (Supplementary Figure 2G). Although this accumulation may result from exaggerated glycolysis and β-oxidation, it may also indicate impaired acetyl disposal as result of a Krebs cycle defects. For +DGF grafts, the latter mechanism is supported by selective and persistent release of the Krebs cycle intermediate α-ketoglutarate (Figure 5c, $P < 0.0005$) as an exclusive feature in these grafts and by an impaired recovery of tissue succinate in the +DGF grafts (Figure 5e).

A final cluster of discriminatory metabolites relates to ongoing cell damage. This cluster includes post-reperfusion release of uracil, an established marker of cell damage[12,13] (Supplementary Figure S3A, $P < 0.0001$) and of amino acid derivates that associate with hydrolysis of plasmalogens (viz. phospho-ethanolamine, ethanolamine, and phospho-serine; Supplementary Figure S3B–D, $P < 0.001$; Supplementary Figure S1). Although no AV differences were present for choline in the +DGF group ($P = 0.60$), this observation is in contrast to a net choline uptake in the living donor and –DGF group ($P < 0.0001$ and 0.02, respectively). Hence, in +DGF grafts, hydrolysis of choline plasmalogens may be masked by choline uptake. Such a mechanism is supported by the selective and progressive release of betaine, the oxidation product of choline[14] in the +DGF group (Supplementary Figures S3G, $P < 0.0001$).

The preceding observations associate incident IRI with persistent post-reperfusion ATP catabolism and ongoing cell damage in a context of mitochondrial failure and activation of

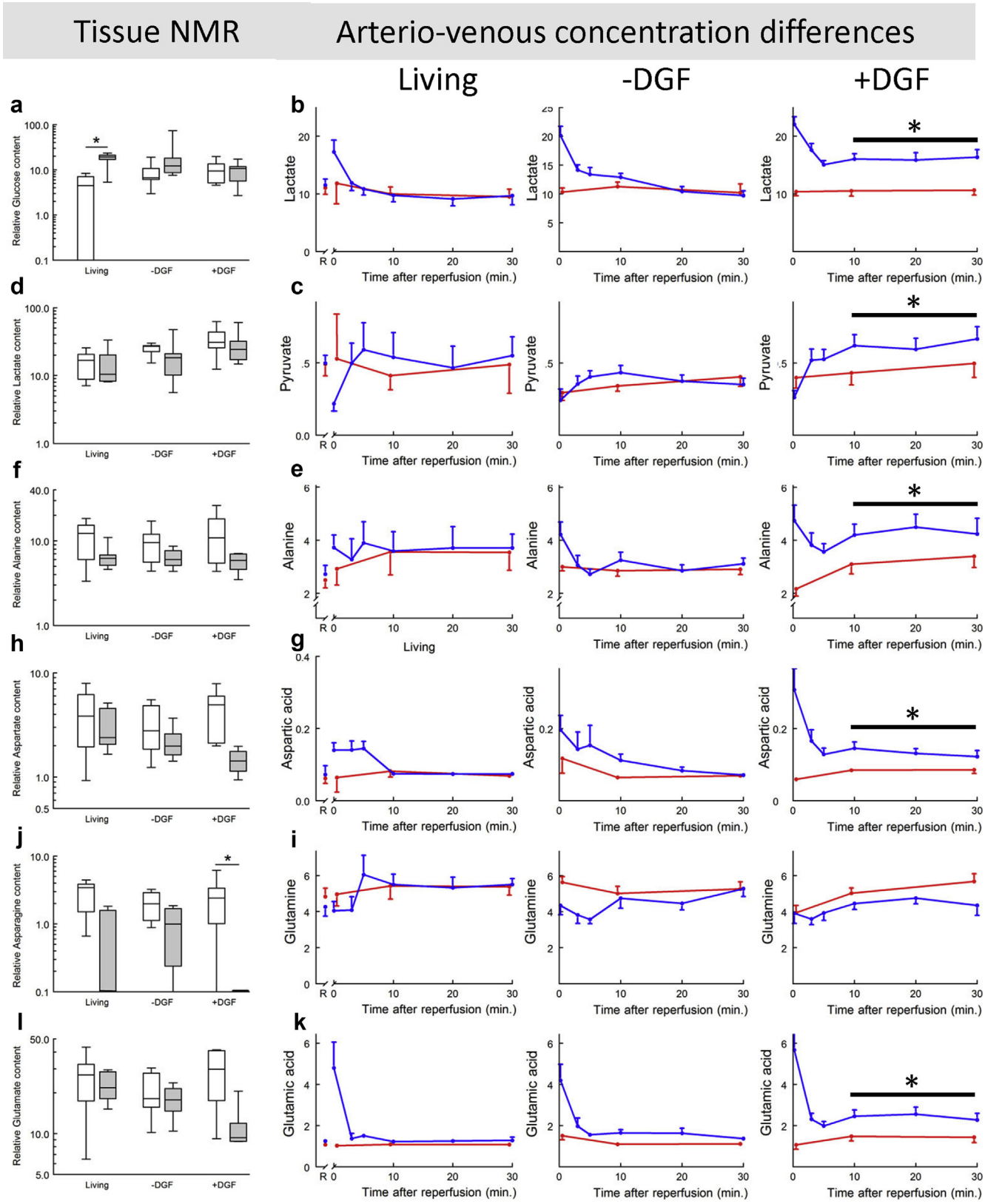

Figure 3 | Post-reperfusion glycolysis and glutaminolysis. Curves for the arterial venous differences (red curve is arterial, blue curve is venous). Tissue biopsies (bar graphs): white bars represent pre-reperfusion biopsies; gray bars represent post-reperfusion biopsies (t = 40 min after reperfusion). *$P < 0.05$. (**a**) Tissue glucose contents. (**b–i**) Glycolysis intermediates: lactate, pyruvate, alanine, aspartate, and asparagine. (**k,l**). Glutaminolysis intermediates glutamine and glutamate. Tissue nuclear magnetic resonance (NMR; $n = 6$ per group): (**a**) tissue glucose recovery in living donor. (**d, f, h**) Stable lactate, alanine, and aspartate tissue contents reflect washout of these intermediates (continued)

glycolytic and lipolytic pathways (Figure 6). Considering the vital role of ATP in cellular homeostasis and survival, it was reasoned that recruitment of auxiliary ATP-regenerative pathways (viz. independent of mitochondrial respiration) would be beneficial. In this context, we considered inosine, a nucleoside that can generate ATP through nontraditional pathways. As shown in Figure 7, neither preventive nor rescue inosine delivery (in concentrations up to 10 mMol/l) rescued ATP exhaustion following chemically induced metabolic paralysis.

DISCUSSION

From this study, performed in the context of clinical kidney transplantation, the picture emerges of IRI (DGF) being a consequence of an almost instantaneous and persistent post-reperfusion failure of oxidative phosphorylation and an activated normoxic glycolysis that is unable to sustain energy homeostasis. In turn, high energy phosphate pools are progressively exhausted, and cellular integrity cannot be preserved, resulting in ongoing tissue damage.

This clinical study is based on integration of metabolic data derived from tissue biopsies taken immediately before and 40 minutes after reperfusion and from sequential assessment of AV differences over the reperfused graft. These AV differences not only provide an indication for the pace and duration of metabolic (mal)adaptions but also allow for directing trends observed in the paired tissue biopsies and for appreciation of metabolite clearance of (e.g., lactate) or uptake from (e.g., medium-chain fatty acids) the circulation.[15,16] The resolution of the AV approach is clearly illustrated by the acylcarnitine data, which not only show selective uptake of medium-chain fatty acids but also suggest that the unsaturated C14 carnitine species tetradecenoyl- and tetradecadienyl carnitine behave similarly to medium-chain fatty acids (Supplementary Data S1) and may not rely on specific fatty acid transporters.[17] In fact, in the process of data analysis, it was observed that sole reliance on tissue biopsies would have obscured most conclusions in this study because the majority of metabolites formed are efficiently cleared into the circulation. Stable arterial blood concentrations show that blood homeostasis is maintained, and consequently metabolites released or absorbed are effectively disposed of or replenished elsewhere.[15,16] Observed stable tissue contents, but clear AV differences challenge the validity of tissue-based metabolomic evaluations. Note that, in the context of deceased donor kidneys and the timeframe of the study, urinary clearance is not an interfering factor because all deceased donor grafts were anuric for the 40-minute measurement interval.

Mapping of the data identifies a metabolic footprint that is fully discriminatory for IRI. Specifically, the reperfusion phase of grafts with future DGF is uniformly and distinctively characterized by severely impaired oxidative phosphorylation (histotoxic hypoxia)[18] and compensatory normoxic glycolysis that is unable to sustain ATP regeneration. The latter conclusion is based on the incomplete recovery of the high-energy phosphate buffer phosphocreatine[19] and on persistent post-reperfusion ATP/GTP catabolism reflected by continued (hypo)xanthine release. In fact, approximation of adenosine losses for +DGF grafts based on hypoxanthine release (AV differences) in the 30 minutes after reperfusion (approximation based on reported post-reperfusion flow rates,[20] average kidney tissue mass,[21] and renal ATP contents[22]) suggests near exhaustion of graft ATP pool 30 minutes post-reperfusion. Critical exhaustion of the ATP pool may result in a catabolic lockdown that renders the cell irresponsive to reestablishment of the proton-motive forces that drive ATP generation, rendering the cell unresponsive to rescue strategies.

The post-reperfusion ATP deficit and histotoxic hypoxia in +DGF grafts may underlie the selective release of amino acids associated with hydrolysis of phospholipids (plasmalogens) in +DGF grafts. Experimental studies identified hydrolysis of plasmalogens and phospholipids as an early characteristic of tissue hypoxia,[23] and hydrolysis of plasmalogens has been described in the context of ischemic kidney injury.[24] Mechanistically, this phenomenon has been linked to membrane translocation and activation of a cytosolic calcium-independent phospholipase A2 resulting from hypoxia-driven complex formation between phospholipase and a phosphofructokinase regulatory element.[25,26] Reversal of hypoxia or ATP treatment dissociates the phospholipase-phosphofructokinase complex and abolishes phospholipase activity. Note that the dynamics of post-reperfusion cessation of (phospho-) ethanolamine release from living donor and –DGF grafts, as well as persistent release in +DGF grafts, may reflect different degrees and rates of metabolic recovery. However, whereas earlier reports imply a role of a cytosolic calcium-independent phospholipase A2,[25,26] observed AV differences for betaine and (phospho-)ethanolamine imply a more comprehensive activation of phospholipases that also involves type C-phospolipases (phospho-ethanolamine) and D-phospolipases (ethanolamine/choline). Similarly, depletion of tissue asparagine (Figure 4j) and release of aspartate (Figure 4g) from +DGF grafts may reflect impaired asparagine synthase activity due to ATP depletion.

Figure 3 (continued) from the kidney. (**j**) Unmeasurable tissue asparagine in + delayed graft function (DFG) post-reperfusion biopsies. Arterial-venous (AV) concentration differences ($n = 10$, 10, and 16 in the living, –DGF, and +DGF groups, respectively): (**b,c**) persistent post-reperfusion lactate ($P < 0.0001$) and pyruvate ($P < 0.04$) release from + delayed graft function (DGF grafts indicating normoxic glycolysis in these grafts. (**e**) Alanine ($P < 0.02$), (**g**) aspartic acid ($P < 0.0001$), and (**k**) glutamate release ($P < 0.002$) from +DGF grafts indicate ongoing glutamine oxidation in these grafts. No significant AV differences were observed for glutamine (**i**).

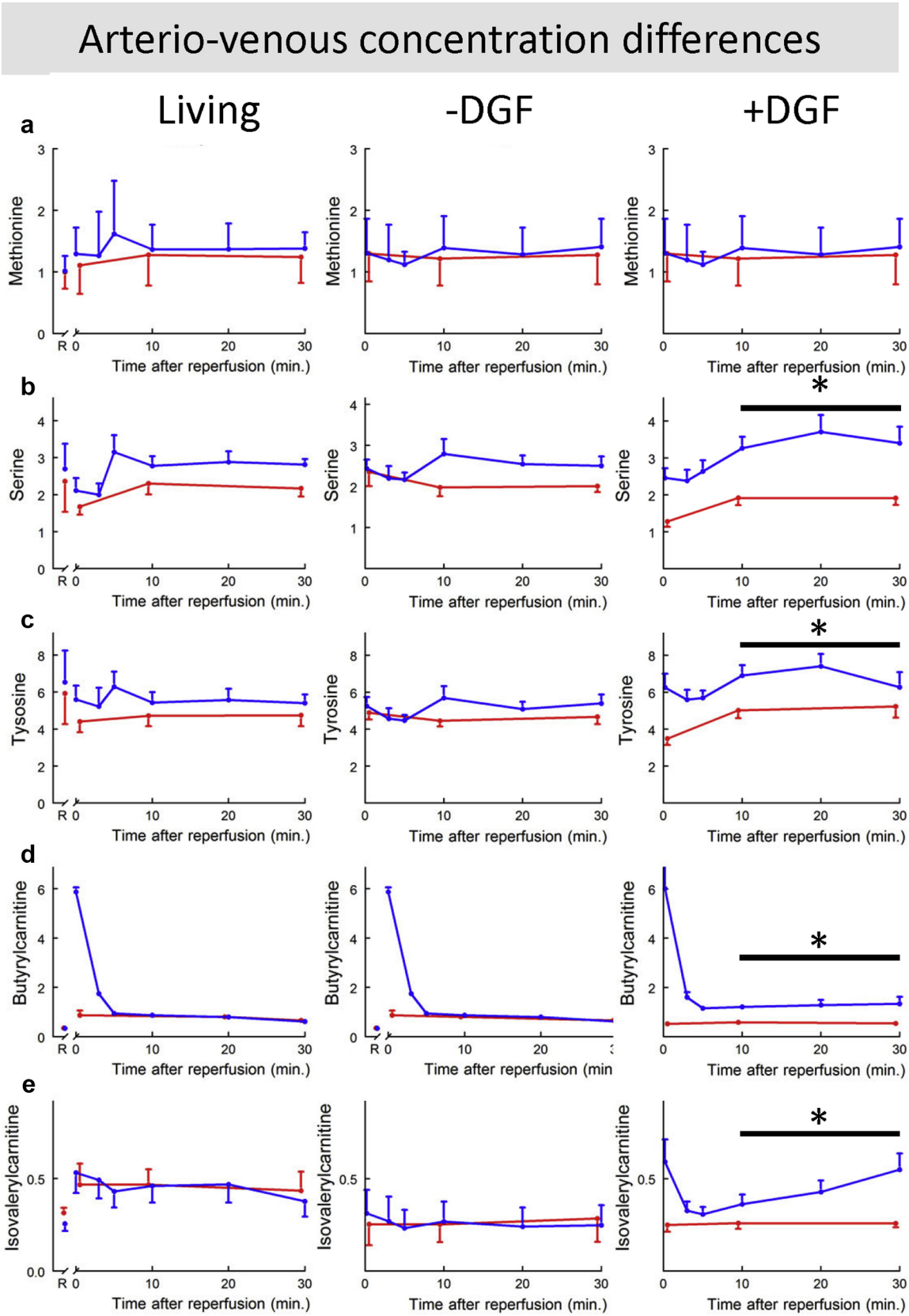

Figure 4 | Activated post-reperfusion autophagia in + delayed graft function (DGF) grafts. Curves for the arterial-venous differences (red curve is arterial, blue curve is venous). Tissue biopsies (bar graphs): white bars represent pre-reperfusion biopsies; gray bars represent post-reperfusion biopsies (t = 40 min after reperfusion). *$P < 0.05$. (**a–c**) Post-reperfusion release of the methionine, serine, and tyrosine (continued)

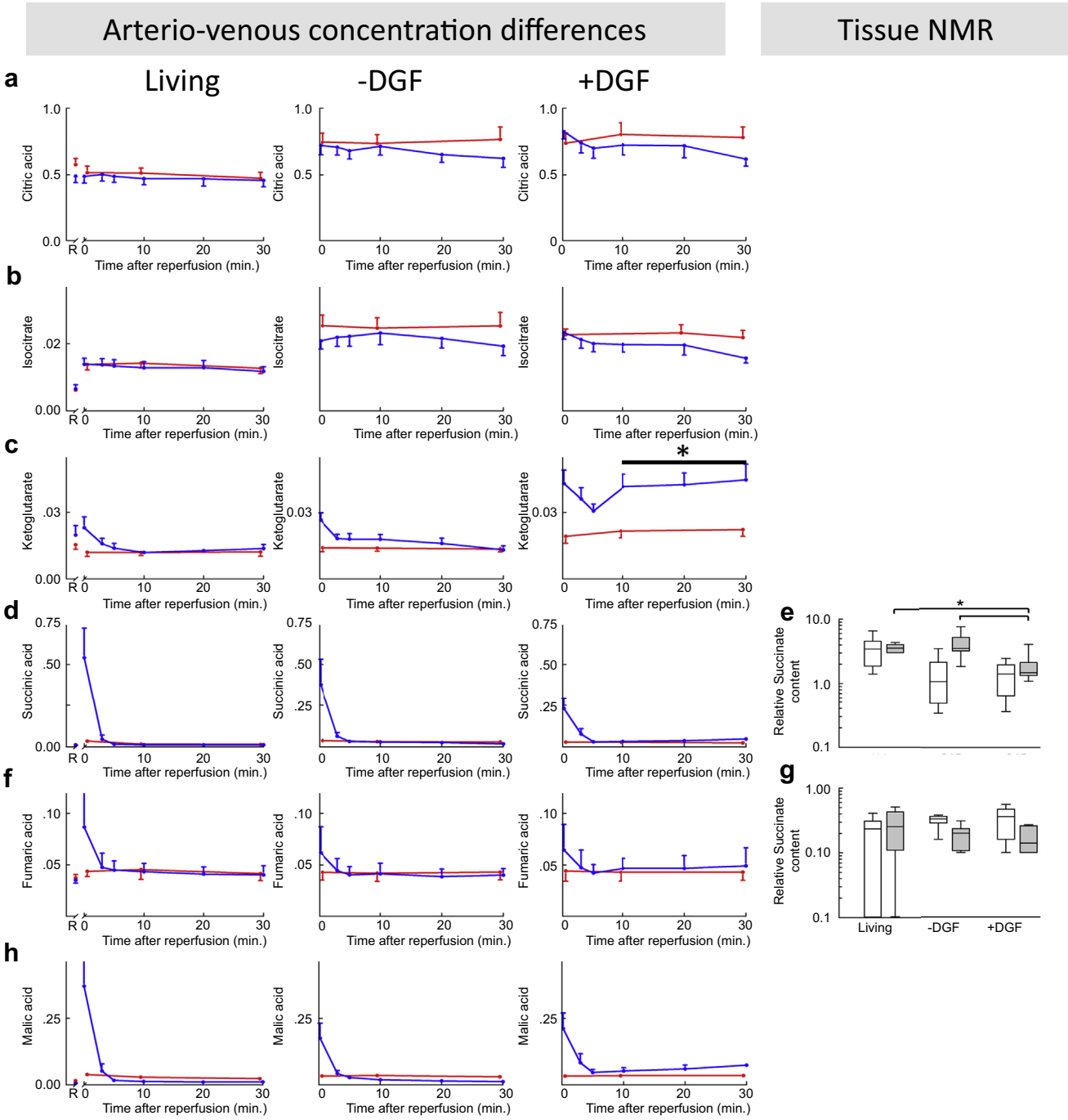

Figure 5 | Post-reperfusion Krebs cycle defect in grafts with future delayed graft function (DGF). Curves for the arterial-venous concentration (AV) differences (red curve is arterial, blue curve is venous). Tissue biopsies (bar graphs): white bars represent pre-reperfusion biopsies; gray bars represent post-reperfusion biopsies (t = 40 min after reperfusion). *$P < 0.05$. (**a–h**) AV differences for the Krebs cycle intermediates ($n = 10$, 10, and 16 in the living, –DGF, and +DGF groups, respectively): persistent release of α-ketoglutarate (from +DGF grafts; $P < 0.001$). (**e,g**) Absent post-reperfusion tissue succinate recovery in +DGF grafts ($P < 0.03$).

Post-reperfusion ATP catabolism in +DGF grafts occurred despite comprehensive activation of catabolic pathways: glycolysis, β-oxidation of medium-chain fatty acids (uniformly activated in all graft types), glutaminolysis (also transiently activated upon reperfusion in living donor and –DGF grafts), and activated autophagy. In fact, post-

Figure 4 (continued) ($P < 0.0002$, 2.10E-6, and 0.0005, respectively) from + DGF grafts ($n = 10$, 10, and 16 in the living, –DGF, and +DGF groups, respectively). (**d,e**) Release of butyryl carnitine ($P < 0.003$) and progressive isovaleryl-carnitine release ($P < 0.006$) from +DGF grafts showing oxidation of branched chain amino acids in the grafts.

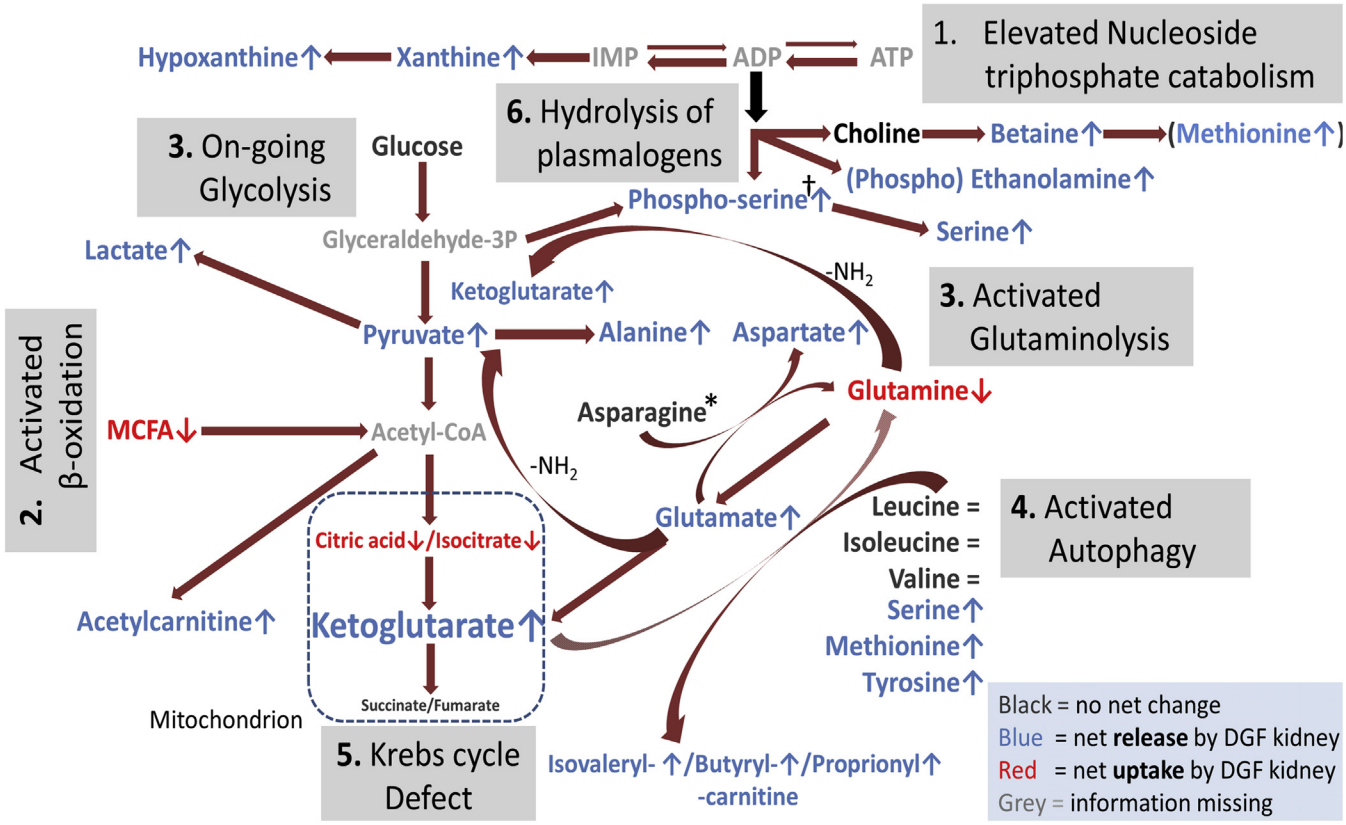

Figure 6 | Unabridged model of the metabolome of renal ischemia reperfusion injury. Metabolites in blue indicate net release from the graft. Metabolites in red indicate net uptake by the graft (arterial-venous concentration [AV] differences). Black = no AV differences; gray = information not available. The 6 metabolic clusters are indicated: (1) nucleoside triphosphate catabolism; (2) β-oxidation (uptake of medium-chain fatty acids [MCFA]); (3) glycolysis/glutaminolysis (pyruvate/lactate release; glutamine uptake and alanine release); (4) autophagy (release of serine, methionine, and tyrosine and of the oxidation products proprionyl-, butyryl-, and isovaleryl-carnitine); (5) Krebs cycle defects—(iso) citrate uptake but ketoglutarate release, and (6) cell damage: release of (phospho-)ethanolamine, betaine, and phospho-serine, implying hydrolysis of plasmalogens.

reperfusion release of isovaleryl- and butyrylcarnitine, deamination products of the branched-chain amino acids isoleucine and leucine,[11] were identified as discriminatory biomarkers for future DGF.

Persistent release of acetylcarnitine and pyruvate from +DGF grafts shows that fluxes created by the activated catabolic pathways exceeded the oxidative capacity. Post-reperfusion ketoglutarate release, net uptake of its precursors citrate and isocitrate from the circulation, and failing tissue succinate recovery imply that the impaired oxidative phosphorylation involves a defect at the level of the oxoglutarate dehydrogenase complex. Specifically, the observed metabolic footprint and the timeframe of the metabolic disturbances do not indicate a role for reversed directability of the Krebs cycle[27,28] in persistent metabolic dysregulation, providing further evidence that the observed mechanism for IRI in rodents[28] does not fully translate to the human context.[29]

Impaired oxoglutarate dehydrogenase activity may be caused by ischemia-related damage to the complex[30] but may also involve, or be exaggerated by, impaired post-reperfusion availability of its cofactors acetyl-coenzyme A, FAD^+, and NAD^+.[31] For +DGF grafts, such deficiencies could occur because of post-reperfusion acetyl-coenzyme A washout and a compromised cellular redox status (reductive stress with impaired NAD^+ availability), a notion supported by the low lactate-to-pyruvate ratio in +DGF grafts.[32]

This metabolic approach does not allow for evaluation of respiratory chain involvement. However, we earlier identified ischemia reperfusion-related defects in both respiratory complex I and II.[7,29] On the basis of the data in this study and previous mitochondrial work, a picture emerges of clinical renal IRI being a consequences of a primary (or eliciting) insult(s) to the mitochondrial Krebs cycle-redox shuttle that occurs before or within the first minutes of reperfusion. Failure to restore ATP levels results in a sustained and comprehensive activation of catabolic pathways, which perpetuates the energy crisis by progressively exhausting the cellular NAD^+ and FAD^+ pool (reductive stress).[33] In this specific context of failing mitochondrial respiration, the purine inosine may be beneficial. Unlike adenosine,[34] inosine is stable in plasma; it has been identified as an alternate source

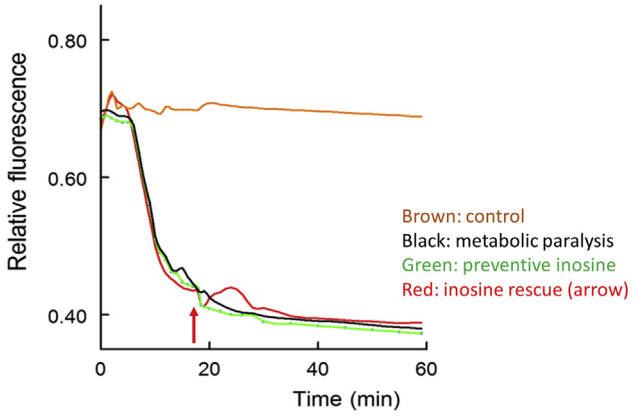

Figure 7 | Both preventive and rescue inosine treatment fail to recover adenosine triphosphate (ATP) levels. The PK-1 renal cell line was stably transfected with the PercevalHR fluorescent biosensor of ATP-to–adenosine diphosphate (ADP) ratio. Chemically induced metabolic-paralysis was induced by adding rotenone/actinomycin/2-deoxyglucose, and the ATP-to-ADP ratio (relative fluorescence) was monitored. Brown, control; black, metabolic paralysis control; green, preventive inosine treatment (10 mMol/l); red, inosine rescue at t = 15 minutes after the induction of a metabolic paralysis.

of ATP in obligatory glycolytic cells (i.e., cells lacking mitochondria) such as erythrocytes[35] and in hypoxic renal cells[36] and is exhausted following reperfusion. Unfortunately, inosine supplementation did not rescue cellular ATP depletion after a forced metabolic shutdown, leaving little room for metabolic rescue strategies aimed at quenching IRI, stressing the reliance on preventive strategies for limiting IRI.

There are limitations to this study. Owing to the large number of comparisons, the potential for significant findings due to random chance in the setting of multiple comparisons is high. Although our conclusions are supported by sound biological relationships, the results may be confounded by issues related to multiple comparisons.

A further limitation is that the study is based on clinical samples; as such, clamp freezing required for direct assessment of ATP and redox status was not possible. Because the metabolome observed is clearly distinct from that reported in animal models and it reflects a system failure, we were unable to perform more detailed evaluations in animal models or *ex vivo* systems such as the respirometry system. Results in this study are for the kidney; thus, conclusions for other organs may be different. The relative high donor age in this study is a reflection of the donor population in the Netherlands. Importantly, 10-year transplantation outcomes for the Netherlands are at least equal to countries with younger donors, such as the United States.[37] As expected the majority of +DGF cases were DCD grafts. We noticed similar metabolic profiles for DBD and DCD grafts; however, the power of this explorative study is obviously too low to detect subtle differences between these 2 donor types.

In conclusion, this study shows that clinical renal IRI is preceded by an almost instantaneous metabolic collapse and an accompanying high-energy phosphate crisis. This deep and persistent metabolic deficit and its instantaneous nature (and consequent minimal window of therapeutic opportunity) will interfere with any pharmaceutical intervention that relies on the availability of ATP. This may explain the poor translatability of preclinical findings to the clinical setting.[2–4] The observed metabolome of clinical DGF sharply contrasts with reported metabolic responses for rats,[28] mice,[38] and pigs,[39,40] which all indicate reinstatement of oxidative phosphorylation within minutes of reperfusion. This may relate to fundamental differences in mitochondrial or metabolic physiology between rodents and larger mammals (e.g., ischemia-induced succinate accumulation does not occur in human donor kidneys).[29] In this context, it is important to point out that all transplanted kidneys are exposed to ischemia reperfusion and that only a subgroup of grafts develops IRI (DGF). Group allocation (+DGF or –DGF) in this study was performed retrospectively, and thus it discriminates between ischemia reperfusion and IRI. It cannot be excluded that the ischemia reperfusion in experimental models[28,38–40] is insufficient to trigger IRI.

Despite the severe damage sustained, all +DGF grafts ultimately recovered, implying a remarkable recovery potential provided that bridging interventions (e.g., dialysis) are available. Of note, although similar metabolomes for DGF in grafts derived from donors deceased after brain death or cardiac death imply a uniform mechanism, there is contrasting impact of DGF on long-term graft survival for the 2 donor types.[41] In fact, although DGF clearly influences survival of grafts from donors deceased after brain death, it does not in such grafts from cardiac donors. This contrast appears to reflect a superior recovery potential of grafts from cardiac death donors.[41]

METHODS

The Leiden University Medical Center medical ethics committee approved the study protocol. Written informed consent was obtained from each patient. This single-center study included 53 patients who underwent kidney transplantation: 37 underwent deceased donor graft procedures and 16 a living donor procedure. On the basis of clinical outcome (DGF), recipients of deceased donor grafts were allocated to a +DGF group ($n = 16$) or –DGF group ($n = 10$). DGF was defined by the need for dialysis in the first week after transplantation.[6]

The study is based on an integration of metabolomic data obtained from sequential arteriovenous (AV) blood sampling during first half hour of reperfusion, and from paired tissue biopsies collected immediately prior to and 40 minutes after reperfusion.

Sequential AV blood sampling over the graft was performed in 36 patients (Supplementary Table S1A). Renal vein blood samples were collected at 30 s, and 3, 5, 10, 20, and 30 minutes and arterial samples at 0, 10, and 30 minutes after reperfusion.[42] Paired pre- and post-reperfusion renal biopsies were obtained immediately before and 40 minutes after reperfusion from 6 living and 12 deceased donor grafts (Supplementary Table S1B; 1 patient had both biopsies and AV sampled).

Targeted metabolomics analyses were performed using standard operating procedures using established mass spectrometry–based platforms or magic angle nuclear magnetic resonance (tissue biopsies).[43] Metabolites covered by the platforms are summarized in Supplementary Table S1.

The potential of inosine to rescue the metabolic deficit during a metabolic collapse was tested in the proximal tubule cell line (LLC-PK1) stably transfected with the PercevalHR fluorescent ATP-adenosine diphosphate biosensor.[44]

With regard to statistics, heat maps were constructed on the basis of z-scores for each metabolite. Within-group changes in tissue metabolite content were tested by the Mann-Whitney test and between-group differences by the Wilcoxon test. AV differences were estimated by using a linear mixed model. Correction for multiple testing was not performed because all observations were part of theoretical networks. Details regarding patients and methods are provided in the Supplementary Methods.

DISCLOSURE

All authors declared no competing interests.

ACKNOWLEDGEMENTS

The Magnetic Resonance core facility is funded by the Faculty of Medicine at NTNU Trondheim, Norway. This study was funded in part by the Dutch Kidney Foundation (Metabolic Salvage Strategies to Improve Transplant Outcome, project 17O/11).

SUPPLEMENTARY MATERIAL

Supplementary File (PDF)

Supplementary Patients and Methods.

Table S1. Patient and transplantation characteristics of the procedures in which paired tissue biopsies were collected (**A**) and in which AV sampling was performed (**B**).

Table S2. Platforms and their metabolites used for AV samples.

Figure S1. Full metabolomic data.

Figure S2. Reinstatement of β-oxidation (medium-chain fatty acids) after reperfusion.

Figure S3. Selective and persistent post-reperfusion washout of uracil and phospholipid (plasmalogen)-associated amino acids from grafts with future DGF.

Data Supplement 1. Raw AV data for the acetyl carnitine, organic acids, and amino acid platforms.

Data Supplement 2. Raw AV data for the purine and pyrimidine platform.

REFERENCES

1. Gutteridge JMC, Halliwell B. Reactive species in disease: friends or foes? In: Halliwell B, Gutteridge JMC, eds. *Free Radicals in Biology and Medicine*. Oxford, UK: Oxford University Press; 2015:511–638.
2. Davidson SM, Ferdinandy P, Andreadou I, et al. Multitarget strategies to reduce myocardial ischemia/reperfusion injury: JACC review topic of the week. *J Am Coll Cardiol*. 2019;73:89–99.
3. Lefer DJ, Bolli R. Development of an NIH consortium for preclinicAl AssESsment of CARdioprotective therapies (CAESAR): a paradigm shift in studies of infarct size limitation. *J Cardiovasc Pharmacol Ther*. 2011;16:332–339.
4. Cavaillé-Coll M, Bala S, Velidedeoglu E, et al. Summary of FDA workshop on ischemia reperfusion injury in kidney transplantation. *Am J Transplant*. 2013;13:1134–1148.
5. Schröppel B, Legendre C. Delayed kidney graft function: from mechanism to translation. *Kidney Int*. 2014;86:251–258.
6. Mallon DH, Summers DM, Bradley JA, et al. Defining delayed graft function after renal transplantation: simplest is best. *Transplantation*. 2013;96:885–889.
7. Wijermars LG, Schaapherder AF, de Vries DK, et al. Defective postreperfusion metabolic recovery directly associates with incident delayed graft function. *Kidney Int*. 2016;90:181–191.
8. Zhang J, Fan J, Venneti S, et al. Asparagine plays a critical role in regulating cellular adaptation to glutamine depletion. *Mol Cell*. 2014;56:205–218.
9. Holecek M. Relation between glutamine, branched-chain amino acids, and protein metabolism. *Nutrition*. 2002;18:130–133.
10. Newgard CB, An J, Bain JR, et al. A branched-chain amino acid–related metabolic signature that differentiates obese and lean humans and contributes to insulin resistance. *Cell Metab*. 2009;9:311–326.
11. Drake KJ, Sidorov VY, McGuinness OP, et al. Amino acids as metabolic substrates during cardiac ischemia. *Exp Biol Med (Maywood)*. 2012;237:1369–1378.
12. De Jong JW, Huizer T, Janssen M, et al. High-energy phosphates and their catabolites. In: Piper HM, Preusse CJ, eds. *Ischemia-Reperfusion in Cardiac Surgery*. Dordrecht, the Netherlands: Springer; 1993:295–315.
13. van Os S, de Abreu R, Hopman J, et al. Purine and pyrimidine metabolism and electrocortical brain activity during hypoxemia in near-term lambs. *Pediatr Res*. 2004;55:1018–1025.
14. Blom HJ, De Vriese AS. Why are homocysteine levels increased in kidney failure? A metabolic approach. *J Lab Clin Med*. 2002;139:262–268.
15. Ivanisevic J, Elias D, Deguchi H, et al. Arteriovenous blood metabolomics: a readout of intra-tissue metabostasis. *Sci Rep*. 2015;5:12757.
16. Jang C, Hui S, Zeng X, et al. Metabolite exchange between mammalian organs quantified in pigs. *Cell Metab*. 2019;30:594–606.
17. Bremer J. Carnitine-metabolism and functions. *Physiol Rev*. 1983;63:1420–1466.
18. Siggaard-Andersen O, Fogh-Andersen N, Gøthgen IH, Larsen VH. Oxygen status of arterial and mixed venous blood. *Crit Care Med*. 1995;23:1284–1293.
19. Stoica SC. High-energy phosphates and the human donor heart. *J Heart Lung Transplant*. 2004;23:S244–S246.
20. Lisik W, Gontarczyk G, Kosieradzki M, et al. Intraoperative blood flow measurements in organ allografts can predict postoperative function. *Transplant Proc*. 2007;39:371–372.
21. Molina DK, DiMaio VJ. Normal organ weights in men: part II—the brain, lungs, liver, spleen, and kidneys. *Am J Forensic Med Pathol*. 2012;33:368–372.
22. Hems DA, Brosnan JT. Effects of ischaemia on content of metabolites in rat liver and kidney in vivo. *Biochem J*. 1970;120:105–111.
23. De Medio GE, Goracci G, Horrocks LA, et al. The effect of transient ischemia on fatty acid and lipid metabolism in the gerbil brain. *Ital J Biochem*. 1980;29:412–432.
24. Rao S, Walters KB, Wilson L, et al. Early lipid changes in acute kidney injury using SWATH lipidomics coupled with MALDI tissue imaging. *Am J Physiol Renal Physiol*. 2016;310:F1136–F1147.
25. Portilla D, Shah SV, Lehman PA, et al. Role of cytosolic calcium-independent plasmalogen-selective phospholipase A2 in hypoxic injury to rabbit proximal tubules. *J Clin Invest*. 1994;93:1609–1615.
26. Hazen SL, Wolf MJ, Ford DA, Gross RW. The rapid and reversible association of phosphofructokinase with myocardial membranes during myocardial ischemia. *FEBS Lett*. 1994;339:213–216.
27. Chinopoulos C. Which way does the citric acid cycle turn during hypoxia? The critical role of α-ketoglutarate dehydrogenase complex. *J Neurosci Res*. 2013;91:1030–1043.
28. Chouchani ET, Pell VR, Gaude E, et al. Ischaemic accumulation of succinate controls reperfusion injury through mitochondrial ROS. *Nature*. 2014;515:431–435.
29. Wijermars LG, Schaapherder AF, Kostidis S, et al. Succinate accumulation and ischemia-reperfusion injury: of mice but not men, a study in renal ischemia-reperfusion. *Am J Transplant*. 2016;16:2741–2746.
30. Tretter L, Adam-Vizi V. Alpha-ketoglutarate dehydrogenase: a target and generator of oxidative stress. *Philos Trans R Soc Lond B Biol Sci*. 2005;360:2335–2345.
31. Heikal AA. Intracellular coenzymes as natural biomarkers for metabolic activities and mitochondrial anomalies. *Biomark Med*. 2010;4:241–263.
32. Sun F, Dai C, Xie J, et al. Biochemical issues in estimation of cytosolic free NAD/NADH ratio. *PLoS One*. 2012;7:e34525.

33. Yu Q, Lee CF, Wang W, et al. Elimination of NADPH oxidase activity promotes reductive stress and sensitizes the heart to ischemic injury. *J Am Heart Assoc*. 2014;3:e000555.
34. Ramakers BP, Pickkers P, Deussen A, et al. Measurement of the endogenous adenosine concentration in humans in vivo: methodological considerations. *Curr Drug Metab*. 2008;9:679–685.
35. Wiback SJ, Palsson BO. Extreme pathway analysis of human red blood cell metabolism. *Biophys J*. 2002;83:808–818.
36. Szoleczky P, Módis K, Nagy N, et al. Identification of agents that reduce renal hypoxia-reoxygenation injury using cell-based screening: purine nucleosides are alternative energy sources in LLC-PK1 cells during hypoxia. *Arch Biochem Biophys*. 2012;517:53–70.
37. Schaapherder A, Wijermars LGM, de Vries DK, et al. Equivalent long-term transplantation outcomes for kidneys donated after brain death and cardiac death: conclusions from a nationwide evaluation. *EClinicalMedicine*. 2018;4(5):25–31.
38. Wei Q, Xiao X, Fogle P, et al. Changes in metabolic profiles during acute kidney injury and recovery following ischemia/reperfusion. *PLoS One*. 2014;9:e106647.
39. Keller AK, Jorgensen TM, Ravlo K, et al. Microdialysis for detection of renal ischemia after experimental renal transplantation. *J Urol*. 2009;182(suppl 4):1854–1859.
40. Fonouni H, Esmaeilzadeh M, Jarahian P, et al. Early detection of metabolic changes using microdialysis during and after experimental kidney transplantation in a porcine model. *Surg Innov*. 2011;18:321–328.
41. de Kok MJ, McGuinness D, Shiels PG, et al. The neglectable impact of delayed graft function on long-term graft survival in kidneys donated after circulatory death associates with superior organ resilience. *Ann Surg*. 2019;270:877–883.
42. de Vries DK, Wijermars LGM, de Vries DK, et al. Early renal ischemia-reperfusion injury in humans is dominated by IL-6 release from the allograft. *Am J Transplant*. 2009;9:1574–1584.
43. Beckonert O, Keun HC, Ebbels TM, et al. Metabolic profiling, metabolomic and metabonomic procedures for NMR spectroscopy of urine, plasma, serum and tissue extracts. *Nat Protoc*. 2007;2:2692–2703.
44. Tantama M, Martínez-François JR, Mongeon R, et al. Imaging energy status in live cells with a fluorescent biosensor of the intracellular ATP-to-ADP ratio. *Nat Commun*. 2013;4:2550.